In-silico CT lung phantom generated from finite-element mesh

Sunder Neelakantan[a], Tanmay Mukherjee[a], Bradford J Smith[b,c], Kyle Myers[d], Rahim Rizi[e], and Reza Avazmohammadi[a,f,g,*]

[a]Department of Biomedical Engineering, Texas A&M University, College Station, TX, USA
[b]Department of Bioengineering, University of Colorado Denver | Anschutz Medical Campus, Aurora, CO, USA
[c]Department of Pediatric Pulmonary and Sleep Medicine, School of Medicine, University of Colorado, Aurora, CO, USA
[d]Hagler Institute for Advanced Study, Texas A&M University, College Station, TX, USA
[e]Department of Radiology, Perelman School of Medicine, University of Pennsylvania, Philadelphia, PA, USA
[f]J. Mike Walker '66 Department of Mechanical Engineering, Texas A&M University, College Station, TX, USA
[g]Department of Cardiovascular Sciences, Houston Methodist Academic Institute, Houston, TX, USA

ABSTRACT

Several lung diseases lead to alterations in regional lung mechanics, including ventilator- and radiation-induced lung injuries. Such alterations can lead to localized underventilation of the affected areas, resulting in the overdistension of the surrounding healthy regions. Thus, there has been growing interest in quantifying the dynamics of the lung parenchyma using regional biomechanical markers. Image registration through dynamic imaging has emerged as a powerful tool to assess lung parenchyma's kinematic and deformation behaviors during respiration. However, the difficulty in validating the image registration estimation of lung deformation, primarily due to the lack of ground-truth deformation data, has limited its use in clinical settings. To address this barrier, we developed a method to convert a finite-element (FE) mesh of the lung into a phantom computed tomography (CT) image, advantageously possessing ground-truth information included in the FE model. The phantom CT images generated from the FE mesh replicated the geometry of the lung and large airways that were included in the FE model. Using spatial frequency response, we investigated the effect of "imaging parameters" such as voxel size (resolution) and proximity threshold values on image quality. A series of high-quality phantom images generated from the FE model simulating the respiratory cycle will allow for the validation and evaluation of image registration-based estimations of lung deformation. In addition, the present method could be used to generate synthetic data needed to train machine-learning models to estimate kinematic biomarkers from medical images that could serve as important diagnostic tools to assess heterogeneous lung injuries.

Keywords: CT imaging, lung phantom, in-silico phantom, image registration

1. INTRODUCTION

There has been growing interest in regional biomarkers to quantify the health of lung parenchyma.[1] Image registration through the use of dynamic imaging has emerged as a powerful tool to assess the kinematic behavior of lung parenchyma during respiration.[2–6] The regional kinematic biomarkers, presented by strain and distortion, offer to provide information about potential sites of lung injuries.[7] Such biomarkers become especially important

Further author information: (Send correspondence to R.A.)
R.A.: E-mail: rezaavaz@tamu.edu, Telephone: 979-862-6521

Medical Imaging 2024: Image-Guided Procedures, Robotic Interventions, and Modeling, edited by Jeffrey H. Siewerdsen, Maryam E. Rettmann, Proc. of SPIE Vol. 12928, 1292829 · © 2024 SPIE · 1605-7422 · doi: 10.1117/12.3006973

in diseases with spatially heterogeneous lung dysfunction and injuries, such as lung inflammation,[8,9] ventilator-induced lung injuries (VILI),[10–12] and radiation-induced lung injury (RILI).[13,14]

One major limitation of the regional strain biomarkers provided by image registration is that they cannot be validated in vivo, especially in the bulk of the parenchyma. The difficulty in validating motion calculations, estimated by image registration, against potential ground truth has limited its use in clinical settings. To address this limitation, studies have used in-vitro gel phantoms,[15–17] which are physically deformed through actuators and imaged using computed tomography (CT) or magnetic resonance (MR) imaging. Subsequently, image registration is performed on the resulting phantom images and compared to the actuator-defined deformation. A common limitation of in-vitro phantoms is perhaps the idealized geometry and motion of the phantom, compared to realistic lung physiology, and potential erroneous displacement and strain estimations in the bulk of the phantom. Indeed, in-vitro phantom validations may be limited to comparing surface strains during physiologically realistic deformation or to simple loading conditions where the bulk can be estimated analytically.

To overcome this barrier, we used a finite-element (FE) lung mesh to generate an in-silico CT phantom. The advantage of an FE model is that it can replicate realistic lung deformation, thus serving as ground-truth measures for strain biomarkers estimated through image registration. Using spatial frequency response, we investigated the effect of "imaging parameters" such as voxel size (resolution) and proximity threshold values on synthesized image quality. In the future, a series of such phantoms generated through in-silico simulation of respiration can be used to perform image registration, and the predicted strains can be compared against the results obtained from the in-silico simulations. Thus, we can use this method to verify the accuracy of various image registration algorithms and choose an optimal method to be used in clinical settings. This method can also be used to investigate the effect of imaging parameters on the results predicted by image registration.

2. METHODS

2.1 Segmentation and reconstruction of FE mesh from CT scan images

The left lung and central airway were reconstructed from CT scans of human lungs (n=1) at end-expiration using Materialise Mimics software. The images were obtained from the EMPIRE10 challenge data set.[18] The segmented left lung and central airways were reconstructed using 3-Matic (Fig. 1A). The airways were extended synthetically using a fractal tree algorithm adopted from Tawhai et al.[19] (Fig. 1B). The airway lumen and walls were removed from the left lung such that the geometry only contained regions that contained porous parenchymal tissue (Fig. 1C). The geometry was used to create a volumetric mesh comprising linear tetrahedral elements, with the nominal size of the element set to 5 mm.

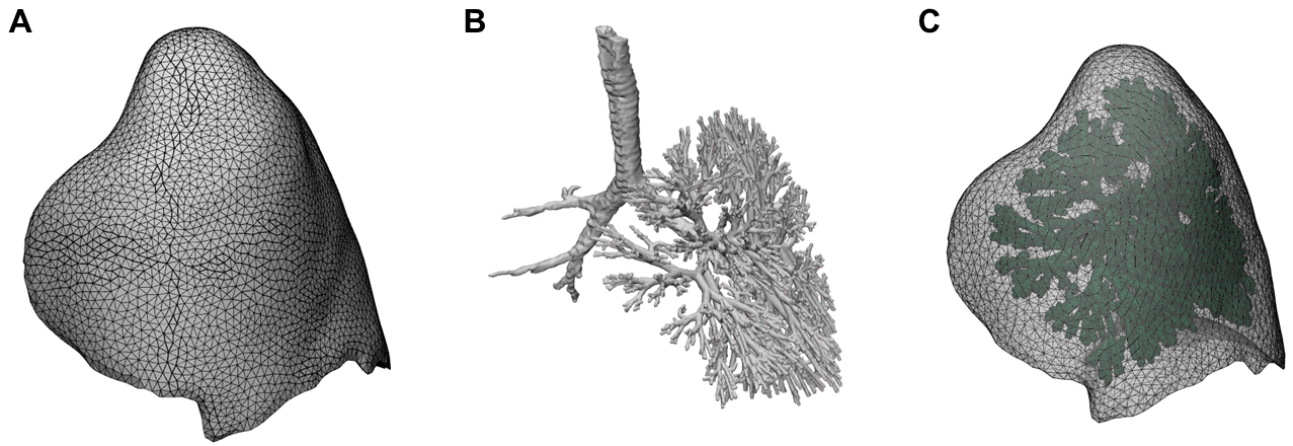

Figure 1. Reconstruction of human lungs. (**A**) Reconstructed left lung. (**B**) Reconstructed central airways and synthetic distal airways. (**C**) Final lung geometry used to generate an in-silico phantom.

2.2 Generation of CT image phantoms from the FE mesh

Following mesh generation, the nodes of the FE lung mesh were mapped onto a uniform visualization toolkit (VTK) grid of predefined parameters. The intensity values of the grid points, which correspond to voxels, were controlled by a proximity threshold, i.e., the number of node points of the mesh within a sphere of a chosen radius centered at a point in the uniform grid. Hence, points on the uniform grid that are close to a large number of FE mesh nodes will be set to high-intensity values. The spatial resolution of the phantoms was controlled by varying the spacing of the uniform grid (reflecting CT image resolution), which corresponds to the voxel size. The final intensity was normalized so that the voxel intensity was between 0 and 1 over the entire image. Finally, the phantoms were exported as .nii (nifty) CT images with grid information (coordinate data, voxel size, resolution, etc.) passed as metadata.

To analyze the variation of phantom quality, we generated phantoms with different voxel size and proximity threshold values. Visual inspection was performed on the phantoms, and the level of details captured in the airways was noted. In addition, to quantify the mesh quality when varying the grid spacing and proximity threshold, the spatial frequency response (SFR) was recorded for each mesh over a single representative slice as the region of interest (ROI). SFR was used as a method to investigate the sharpness and detail in the image by analyzing the distance (spatial frequency) over which voxel intensity values change in a given ROI. SFR curves are a representation of the frequency of intensity changes; a higher SFR value at a lower spatial frequency indicates a large number of gradual changes, which result in blurred but smooth images. Conversely, a higher SFR value at a high frequency indicates a large number of intensity changes over a small distance, leading to a sharper but also jagged image.

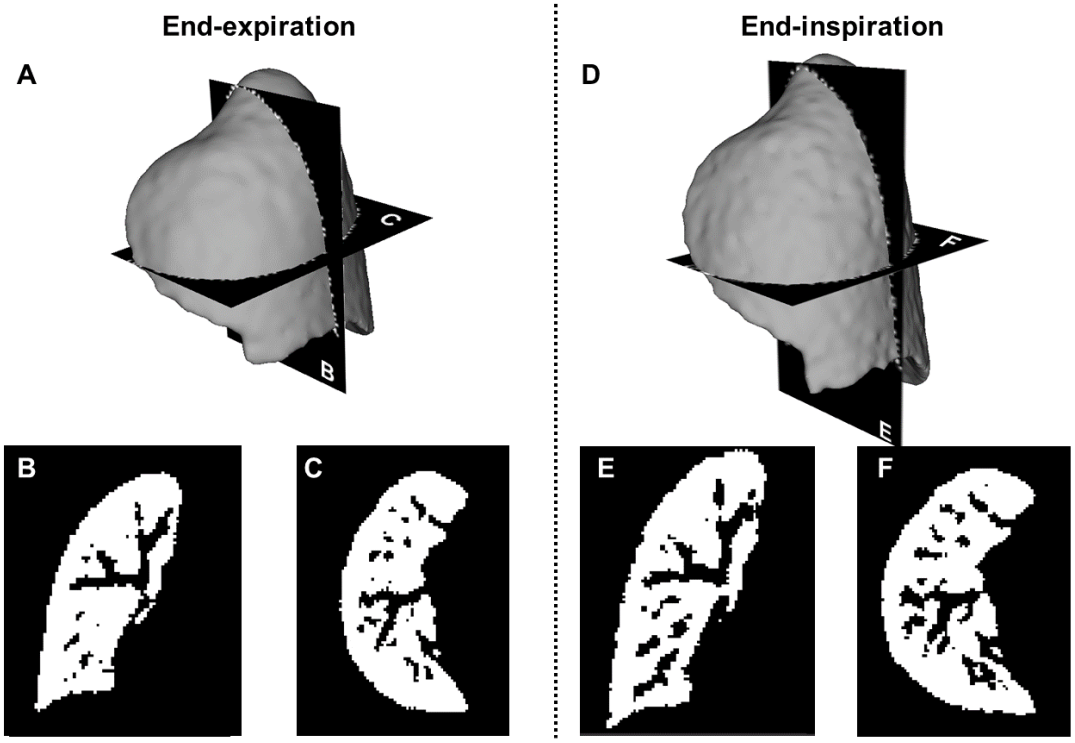

Figure 2. (**A**) Geometry and slices at end-expiration from (**B**) frontal and (**C**) transverse planes. (**D**)Geometry and slices at the end-inspiration from (**E**) frontal and (**F**) transverse planes. End-inspiration mesh was obtained by deforming the end-expiration mesh to simulate inflation. Voxel intensity values were binarized to 0 and 1.

3. RESULTS

The phantom image stack captured the structure of the lungs and the major airways at a voxel size of 2 mm (Fig. 2). The mapping from the unstructured to the structured grid was performed at a proximity threshold of

1.5 mm. The final voxel intensity values were binarized to be either 0 or 1. This method was applied to the FE mesh of the lung at two timepoints in the respiratory cycle, namely, the beginning and the end of inspiration (Figs. 2B,C,E,F). The end-inspiratory mesh was obtained by geometrically deforming the end-expiration mesh, i.e., scaling the mesh by a factor of 1.1, 1.1, 1.3 along the x, y, and z axes, respectively. The number of airway generations captured in the images depended on the prescribed spatial resolution, with smaller airways needing higher resolutions to be present in the images and appearing as isolated empty voxels in the bulk of the lung tissue when the prescribed resolution was not sufficient.

When investigating the effect of voxel size and proximity threshold (Fig. 3), reducing the space between voxels led to a steady increase in image quality and level of detail but also increased the presence of noise. This noise could be due to the non-uniform distribution of node points in the FE mesh, which could be reduced by refining the mesh to contain a more uniform distribution of node points. Conversely, increased values resulted in a complete figure when investigating proximity thresholds, while decreased values led to a sparse point cloud.

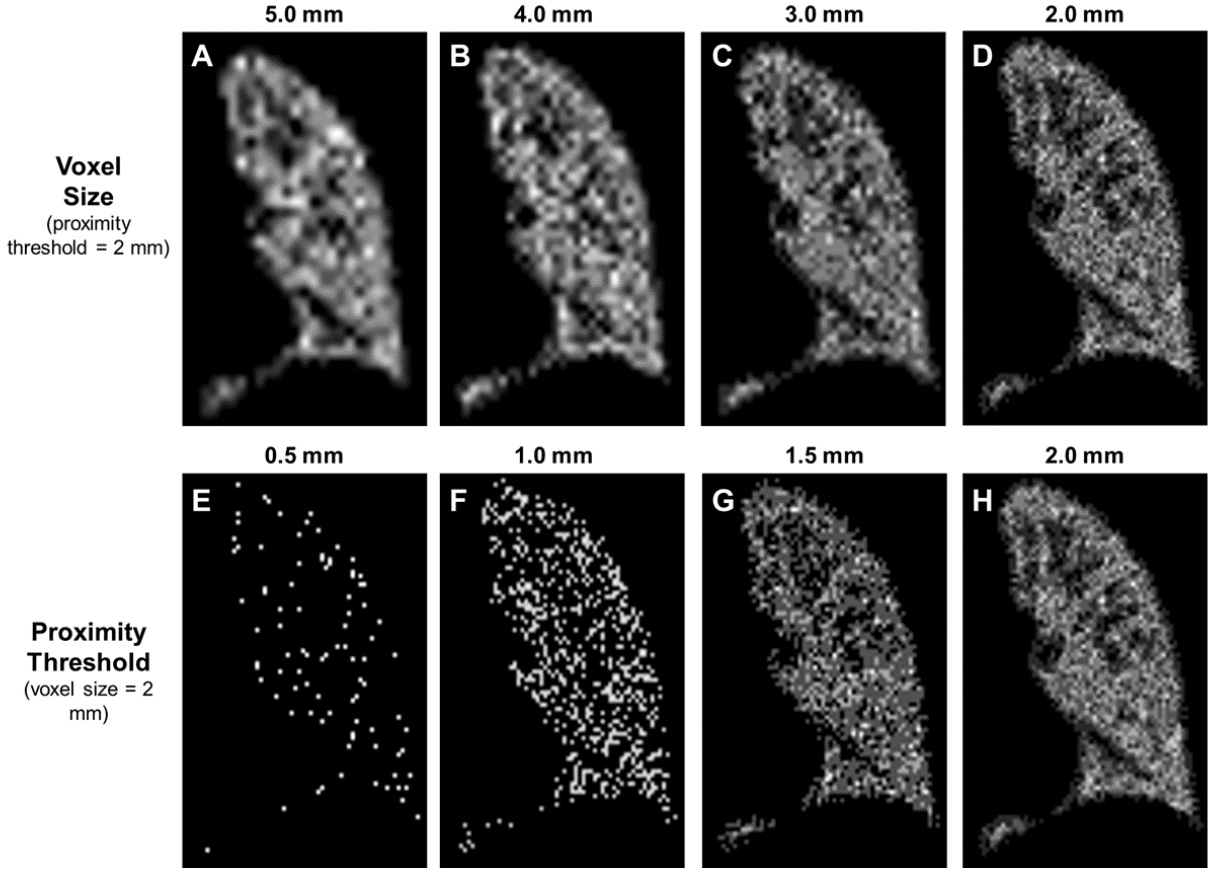

Figure 3. (**A-D**) Variation of voxel size at a fixed proximity threshold. (**E-H**) Variation of proximity threshold at a fixed voxel size. All images were resized to 500 x 800 pixels. Voxel intensity values normalized to be between 0 and 1 for each figure.

The effect of varying voxel size and proximity threshold values was also observed in the SFR curves in a specific ROI (Fig. 4A). When varying voxel size, the SFR curves moved to the left, indicating that there was an increase in a lower frequency response (Fig. 4B). The same behavior was observed when lowering the proximity threshold values (Fig. 4C). The increased lower frequency response indicated that there were fewer sudden shifts in intensity values (white to black or vice versa), i.e., higher frequency response. The results indicated that proximity threshold values had a greater effect on SFR compared to the voxel size.

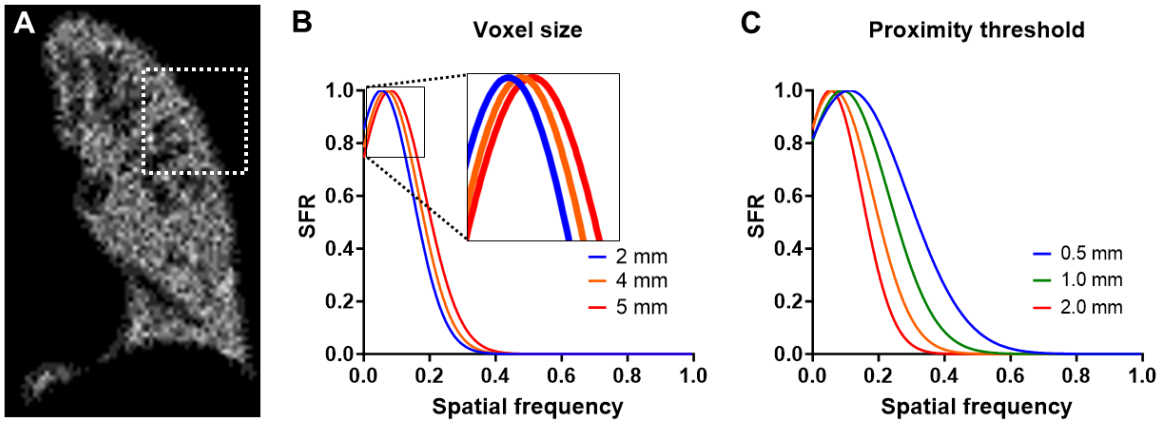

Figure 4. (**A**) Representative slice and region of interest used for spatial frequency response (SFR) analysis. (**B**) Effect of voxel size on SFR. (**C**) Effect of proximity threshold values on SFR. SFR analysis was performed on a resized image of size 500 x 800 pixels.

4. DISCUSSION

In this study, we have reported a method to use the FE mesh of the lungs to generate an in-silico CT image phantom. We observed that the in-silico phantom was able to replicate the lung geometry and architectural detail in the lungs at low values of voxel size. The proximity threshold values could be prescribed based on the mesh to ensure the optimal level of detail for potential image registration purposes. In addition, the variation of voxel size and proximity threshold values can also be used to study the effect of imaging parameters such as resolution and noise in CT images on the kinematic behavior predicted by image registration.

The method presented in this study has several significant applications. Some of these applications in the context of evaluating and improving image registration are detailed below. Our method can be used as an in-silico benchmark to validate image-registration-based estimations of lung deformation. The in-silico phantom can be used to validate and compare different image registration algorithms against a "ground truth," contained in finite-element simulations.[20] Along those lines, the phantom can be used to generate synthetic CT images with a resolution higher than that of the image used to create the FE model. The high-resolution synthesized images can be used as benchmarks to evaluate the accuracy and reproducibility of image registration algorithms.[21] Also, the proposed phantom can be used to generate synthetic data to develop machine-learning surrogates for image registration such that kinematic biomarkers can be quantified through only basic measurements from raw DICOM/Nifty images.[22,23] The use of deep learning to perform image registration in the lungs from raw images has gained increasing popularity in recent times.[5,24] While machine learning models can be trained using publicly available repositories, one limitation is the lack of availability of four-dimensional CT (4DCT) image stacks in human patients. Dynamic CT scans are avoided in human patients due to the high levels of radiation, but this can be overcome by in-silico phantom images that can be generated throughout the respiratory cycle at any prescribed resolution. Our method can serve as an important tool in generating and augmenting training data for machine learning models. In addition, our method can be applied to generate "synthetic" images between two scans, reducing the difference between consecutive images and leading to improved accuracy of image registration tools.

The presence of the smaller airways in phantom images was dependent on the prescribed resolution. This indicates the need to perform the phantom generation at a smaller voxel size, which corresponds to a higher CT resolution. Based on our results, a voxel size of lower than 1 mm is required to capture smaller airways accurately. In addition, the proximity threshold values need to be optimized to reduce the noise, thus enabling the visualization of smaller airways. This work was limited to generating an image stack each from the beginning and end of one inspiratory cycle as a proof of concept. Future studies will involve a deforming mesh and the generation of multiple CT stacks to represent a complete respiratory cycle, thus simulating dynamic 4DCT scans.

The deformation between these phantom images will be analyzed using image registration and compared to the deformation of the original mesh during the in-silico simulation.

5. CONCLUSION

In this study, we have reported a method to use an FE mesh of human lungs to generate a CT image phantom. We expect this study to serve as an important step toward standardizing the validation of voxel-based image registration algorithms and optimizing dynamic imaging parameters for improved image registration accuracy. The validated kinematic biomarkers are expected to improve the diagnosis and risk stratification strategies in patients with chronic or acute lung injuries.

ACKNOWLEDGMENTS

This work was supported by the National Institutes of Health award R00HL138288 and the National Science Foundation award 2244995 to R.A.

REFERENCES

[1] Neelakantan, S. *et al.* Computational lung modelling in respiratory medicine. *Journal of The Royal Society Interface* **19**, 20220062 (2022).

[2] Sotiras, A., Davatzikos, C. & Paragios, N. Deformable medical image registration: A survey. *IEEE Transactions on Medical Imaging* **32**, 1153–1190 (2013).

[3] Bel-Brunon, A., Kehl, S., Martin, C., Uhlig, S. & Wall, W. Numerical identification method for the nonlinear viscoelastic compressible behavior of soft tissue using uniaxial tensile tests and image registration – application to rat lung parenchyma. *Journal of the Mechanical Behavior of Biomedical Materials* **29**, 360–374 (2014).

[4] Hurtado, D. E., Villarroel, N., Retamal, J., Bugedo, G. & Bruhn, A. Improving the accuracy of registration-based biomechanical analysis: A finite element approach to lung regional strain quantification. *IEEE Transactions on Medical Imaging* **35**, 580–588 (2016).

[5] Fu, Y. *et al.* Lungregnet: An unsupervised deformable image registration method for 4D-CT lung. *Medical Physics* **47**, 1763–1774 (2020).

[6] Keshavarzian, M. *et al.* An image registration framework to estimate 3D myocardial strains from cine cardiac mri in mice. In *International Conference on Functional Imaging and Modeling of the Heart*, 273–284 (Springer, 2021).

[7] Neelakantan, S. *et al.* Volumetric versus distortional deformation in rat lungs. In Linte, C. A. & Siewerdsen, J. H. (eds.) *Medical Imaging 2023: Image-Guided Procedures, Robotic Interventions, and Modeling*, vol. 12466, 124661R. International Society for Optics and Photonics (SPIE, 2023).

[8] Cereda, M. *et al.* Imaging the interaction of atelectasis and overdistension in surfactant-depleted lungs*. *Critical Care Medicine* **41** (2013).

[9] Avazmohammdi, R. *et al.* Acute functional adaptation of the right ventricle in ARDS. *Am J Respir Crit Care Med* **203**, A3696 (2021).

[10] Otto, C. M. *et al.* Spatial and temporal heterogeneity of ventilator-associated lung injury after surfactant depletion. *Journal of Applied Physiology* **104**, 1485–1494 (2008).

[11] Jain, S. V. *et al.* The role of high airway pressure and dynamic strain on ventilator-induced lung injury in a heterogeneous acute lung injury model. *Intensive Care Medicine Experimental* **5** (2017).

[12] Herrmann, J., Kollisch-Singule, M., Satalin, J., Nieman, G. F. & Kaczka, D. W. Assessment of Heterogeneity in Lung Structure and Function During Mechanical Ventilation: A Review of Methodologies. *Journal of Engineering and Science in Medical Diagnostics and Therapy* **5**, 040801 (2022).

[13] Travis, E. L., Liao, Z.-X. & Tucker, S. L. Spatial heterogeneity of the volume effect for radiation pneumonitis in mouse lung. *International Journal of Radiation Oncology*Biology*Physics* **38**, 1045–1054 (1997).

[14] Marks, L. B. *et al.* Radiation-induced lung injury. *Seminars in Radiation Oncology* **13**, 333–345 (2003).

[15] Rippey, J. & Gawthrope, I. Creating thoracic phantoms for diagnostic and procedural ultrasound training. *Australasian Journal of Ultrasound in Medicine* **15**, 43–54 (2012).

[16] Zhou, J. & Zhang, X. A lung phantom model to study pulmonary edema using lung ultrasound surface wave elastography. *Ultrasound in Medicine Biology* **44**, 2400–2405 (2018).

[17] Colvill, E. *et al.* Anthropomorphic phantom for deformable lung and liver ct and mr imaging for radiotherapy. *Physics in Medicine Biology* **65**, 07NT02 (2020).

[18] Murphy, K. *et al.* Evaluation of registration methods on thoracic ct: the empire10 challenge. *IEEE transactions on medical imaging* **30**, 1901–1920 (2011).

[19] Tawhai, M. H., Pullan, A. J. & Hunter, P. J. Generation of an anatomically based three-dimensional model of the conducting airways. *Annals of Biomedical Engineering* **28**, 793–802 (2000).

[20] Mukherjee, T. *et al.* In-silico heart model phantom to validate cardiac strain imaging. *preprint* DOI: 10.13140/RG.2.2.12012.33923 (2023).

[21] Mukherjee, T. *et al.* Complete spatiotemporal quantification of cardiac motion in mice through enhanced acquisition and superresolution reconstruction. *preprint* DOI: 10.13140/RG.2.2.14552.26885 (2024).

[22] Babaei, H. *et al.* A machine learning model to estimate myocardial stiffness from EDPVR. *Scientific Reports* **12**, 5433 (2022).

[23] Mehdi, R. R. *et al.* Chapter 19 - comparison of three machine learning methods to estimate myocardial stiffness. In Chinesta, F., Cueto, E., Payan, Y. & Ohayon, J. (eds.) *Reduced Order Models for the Biomechanics of Living Organs*, Biomechanics of Living Organs, 363–382 (Academic Press, 2023).

[24] Xiao, H. *et al.* Deep learning-based lung image registration: A review. *Computers in Biology and Medicine* **165**, 107434 (2023).